Thermodynamic Data for Mn_3O_4, Mn_2O_3 and MnO_2

K.T. Jacob[1*], A. Kumar[1], G. Rajitha[1] and Y. Waseda[2]

[1]*Department of Materials Engineering, Indian Institute of Science, Bangalore 560012, India*

[2] *Institute of Multidisciplinary Research for Advanced Materials, Tohoku University, Sendai 980-8577, Japan*

ABSTRACT

Thermodynamic properties of Mn_3O_4, Mn_2O_3 and MnO_2 are reassessed based on new measurements and selected data from the literature. Data for these oxides are available in most thermodynamics compilations based on older calorimetric measurements on heat capacity and enthalpy of formation, and high-temperature decomposition studies. The older heat capacity measurements did not extend below 50 K. Recent measurements have extended the low temperature limit to 5 K. A reassessment of thermodynamic data was therefore undertaken, supplemented by new measurements on high temperature heat capacity of Mn_3O_4 and oxygen chemical potential for the oxidation of MnO_{1-x}, Mn_3O_4, and Mn_2O_3 to their respective higher oxides using an advanced version of solid-state electrochemical cell incorporating a buffer electrode. Because of the high accuracy now achievable with solid-state electrochemical cells, phase-equilibrium calorimetry involving the "third-law" analysis has emerged as a competing tool to solution and combustion calorimetry for determining the standard enthalpy of formation at 298.15 K. The refined thermodynamic data for the oxides are presented in tabular form at regular intervals of temperature.

---

* Corresponding Author, E-mail: katob @materials.iisc.ernet.in

1. INTRODUCTION

A great deal of attention has been given to the effective utilization of manganese and improved recovery from its ores, which are principally oxides. In manganese oxides, the cations exist in three oxidation states (Mn^{2+}, Mn^{3+} and Mn^{4+}). The oxides MnO_{1-x}, Mn_3O_4, Mn_2O_3 and MnO_2 can be converted from one to another by adjustment of temperature (T) and oxygen partial pressure (P_{O_2}). Manganese in oxidation states of 2^+, 3^+, 4^+ has interesting applications which encompass systems such as $LaMnO_3$-based perovskites and metastable manganese oxides and oxyhydroxides, which are phases encountered in fuel cell, battery, electronic and environmental applications. Thermodynamic properties of binary oxides provide the foundation for measurements and assessments on ternary and higher order oxides.

Thermodynamic properties of manganese oxides and the phase diagram for the system Mn-O were recently assessed by Grundy et al. /1/. An exhaustive compilation of all published data on phase diagram and thermodynamic properties is presented by Grundy et al. They concluded that the Gibbs energy of formation of MnO is known only with large uncertainty (±5 kJ mol^{-1}) and this leads to uncertainties in the Gibbs energies of formation of all other oxides since Gibbs energies of higher oxides are based on data for MnO. Subsequently, Gibbs energy of formation of MnO was measured accurately (±0.25 kJ mol^{-1}) by Jacob et al. /2/, consistent with earlier measurements of Alcock and Zador /3/. In this communication, we combine the accurate data for MnO with new measurements on oxygen chemical potentials of three biphasic regions in the phase diagram of the system Mn-O and high-temperature heat capacity of Mn_3O_4 to derive accurate data for Mn_3O_4, Mn_2O_3 and MnO_2, taking cognizance of other reliable measurements available in the literature including new low temperature heat capacity measurements. For new measurements on oxygen chemical potential, an advanced version of the solid-state cell incorporating a buffer electrode is utilized. Of the four oxides of manganese, only MnO exhibits significant nonstoichiometry at temperatures above 900 K. New experimental data obtained in this study is first presented, followed by reassessment of data for the three higher oxides.

2. EXPERIMENTAL WORK

2.1. Materials

Pure MnO_2 (99.999% pure) was obtained from Johnson Matthey Inc. Mn_2O_3 was prepared by heating MnO_2 in air at 973 K for ~20 ks, and Mn_3O_4 by heating at 1323 K for ~20 ks. Formation of the various phases was confirmed by powder XRD.

2.2. Differential Scanning Calorimetry (DSC)

Since the high-temperature heat capacity of α-Mn_3O_4 has not been reported in the literature, DSC was used to measure this property of under pure argon gas in the temperature range from 350 to 1100 K. The DSC instrument was operated in the step-heating mode to increase accuracy; α-Al2O3 was used as the reference material. The alumina powder was dehydrated via vacuum treatment at 1200 K. The difference in the heat flux into the sample and the reference material was integrated during heating at a constant rate (2 K/min) over small temperature steps (10 K) with an isothermal dwell time of 15 min. The accuracy of the measured heat capacity is estimated to be 1% (2σ). (The standard error estimate is denoted as σ). XRD analysis of the oxide after the DSC experiments did not indicate any change in structure or lattice parameter.

2.3. Oxygen potential measurements

The reversible emfs of three solid-state cells were measured as a function of temperature:

Cell 1: Pt, $Mn_{1-x}O + Mn_3O_4$ // (Y_2O_3) ZrO_2 // O_2 (0.1 MPa), Pt

Cell 2: Pt, $Mn_3O_4 + Mn_2O_3$ // (Y_2O_3) ZrO_2 // O_2 (0.1 MPa), Pt

Cell 3: Pt, $Mn_2O_3 + MnO_2$ // (Y_2O_3) ZrO_2 // O_2 (0.1 MPa), Pt

The cells are written such that the right hand electrodes are positive. Two experiments were conducted on each cell. Yttria-stabilized zirconia, (Y_2O_3) ZrO_2, is an oxygen ion conductor with ionic transport number greater than 0.99 at the temperatures and oxygen partial pressures encountered at the electrodes of the three cells /4/. However, the presence of trace hole conduction in the electrolyte gives rise to a small electrochemical flux of oxygen from the reference electrode on the right side to the working electrodes on the left side of each cell /5/. The electrochemical permeability is caused by the coupled transport of oxygen ions and holes in the solid electrolyte under the oxygen potential gradient.

The electrochemical flux of oxygen can polarize the two-phase solid electrodes. The chemical potential of oxygen in the micro system near the solid electrode/electrolyte interface can be altered because of the semi-permeability of the electrolyte to oxygen. A buffer electrode, introduced between reference and working electrodes can act as a sink for the oxygen flux and prevent the flux from reaching the working electrode. To be effective, the buffer electrode should be maintained at an oxygen chemical potential close to that of the working electrode. Since there is no significant difference between the chemical potentials of buffer and working electrodes, driving force for transport of oxygen through the zirconia tube separating these electrodes does not exist. The working electrode therefore remains unpolarized. Pure oxygen gas at a pressure of 0.1 MPa, flowing over a platinized surface of zirconia, constitutes the primary reference standard for oxygen chemical potential and forms a non-polarizable electrode. Thus, the three-electrode design of the cell prevents error in emf caused by polarization of the working electrode. Measuring separately the emf between the three electrodes, two at a time, can assess the magnitude of the polarization effect. Transport of oxygen between the electrodes through the gas phase is prevented by physical isolation of the gas phase over the three electrodes.

The cell design used for high-temperature emf measurements on cells 1 and 2 is shown schematically in **Figure 1**. It consisted of three distinct compartments, separated by two impervious yttria-stabilized zirconia (YSZ) tubes and a YSZ crucible. An ionic bridge was provided through the buffer electrode. The cell can be represented schematically as follows:

Working Electrode $O_2\,(P'_{O_2})$, Pt	$(Y_2O_3)ZrO_2$ No flux	$(Y_2O_3)ZrO_2$ Buffer Electrode $O_2\,(P''_{O_2})$, Pt/Pd $P''_{O_2} \approx P'_{O_2}$	$(Y_2O_3)ZrO_2$ $\leftarrow$ O^{2-}	Reference Electrode O_2 (0.1 MPa), Pt

The working and reference electrodes were contained inside separate zirconia tubes. The cell emf measured between the working and reference electrodes was determined only by

the oxygen chemical potential at these electrodes and was not affected by the gradient of chemical potential through the connecting chain consisting of the solid electrolyte segments including the ionic bridge across the buffer electrode. Construction of the high-temperature galvanic cell was rendered more difficult by the introduction of the buffer electrode. Moreover, in some of the cells used in this study, the partial pressure of oxygen at the working electrode was quite appreciable, especially at the higher temperatures. Therefore, the static sealed design used by Charette and Flengas /6/ was found more appropriate than other designs that employ either dynamic vacuum or inert gas flow over the electrodes /4,7/.

The working electrodes consisted of a mixture of two adjacent manganese oxides in equimolar ratio. The average particle size of the powders used to prepare the working and buffer electrodes was in the range from 2 to 10 μm. The compositions of the buffer electrodes were identical to that of the corresponding working electrodes.

The details of cell assembly and operational procedures used in this study for cells 1 and 2 were identical with those reported elsewhere /8,9/. The working and buffer electrodes are sealed under vacuum in separate compartments where the equilibrium oxygen partial pressures are established by dissociation of the higher oxide at high temperature. Because of the high dissociation pressure of MnO_2, cell 3 can be operated only at relatively low temperatures. The high internal resistance associated with the cell design shown in Figure 1 does not permit measurements on cell 3 at relatively lower temperatures. Further, there was some evidence in preliminary experiments of formation of PtO_2 as a dilute solution in MnO_2. Hence, a different type of apparatus /10,11/, in which there was no contact between the electrode containing $Mn_2O_3 + MnO_2$ and Pt, was used for measurements on cell 3.

A mixture of Mn_2O_3 and MnO_2 in the molar ration 1:2 was taken in a zirconia crucible, which was placed inside a narrow quartz tube closed at one end. A long tube of yttria-stabilized zirconia, with RuO_2/Pt electrodes attached to the inside and outside surfaces of the closed end, was used to measure the oxygen potential in the gas phase above the sample. The gap between the outer silica tube and the zirconia tube at the cold end was sealed by Dekhotinsky cement. The silica tube housing the cell assembly was evacuated through a side arm and flame sealed under vacuum. Pure oxygen gas was passed through

the inside of the zirconia tube. The cell was suspended inside a vertical furnace. The oxygen molecules generated by the dissociation of MnO_2 to Mn_2O_3 established the equilibrium oxygen pressure inside the silica tube housing the cell. The time required to establish equilibrium oxygen pressure and hence steady emf was of the order of 1.5 Ms.

3. RESULTS

3.1. High-temperature heat capacity of Mn_3O_4

The high-temperature heat capacity of Mn_3O_4 obtained in this study using a differential scanning calorimeter (DSC) is shown in **Figure 2** as a function of temperature. The results can be expressed by the equation:

$$C_P^o \ / \ \mathrm{J\ K^{-1}\ mol^{-1}} = 145.322 + 49.411\mathrm{x}10^{-3}(T/\mathrm{K}) - 1.574\mathrm{x}10^{6}(T/\mathrm{K})^{-2} \qquad (1)$$

in the temperature range from 350 to 1100 K. The authors are not aware of any prior high-temperature heat capacity measurement for comparison with the data obtained in this study.

3.2. Oxygen potentials for $Mn_{1-x}O$–Mn_3O_4, Mn_3O_4–Mn_2O_3 and Mn_2O_3–MnO_2 equilibria

The reversibility of the cells was tested by microcoulometric titration in forward and reverse directions. Since the emf returned to the same value after essentially infinitesimal successive displacements from equilibrium in opposite directions, reversibility was confirmed. The emf was found to be reproducible on temperature cycling. At the end of each experiment, the electrodes were cooled to room temperature and examined by XRD. There was no detectable change in the phase composition of the electrodes during emf measurement.

The reversible emfs of cells 1 and 2 are plotted as a function of temperture in **Figures 3 and 4**, repectively. The emf of cell 1 was positive and could be measured in the temperature range from 850 to 1400 K. The magnitude of the polarization effect, assessed by measuring the emf between the buffer electrode and the other two electrodes, varied from 4 to 6 mV for cell 1 depending on temperature. If the buffer electrode was not used

the measured emf would have been lower by this amount. The emf of cell 1 exhibited a linear dependence on temperature over the extended temperature range, probably because the expected non-linearity due to ΔC_P for the cell reaction is compensated by the variation of nonstoichiometry of MnO_{1-x} with temperature.

The emf of cell 2 exhibited irreversibility below 900 K and became negative at temperatures over 1247 K, indicating that the oxygen pressure over the measuring electrode exceeded atmospheric pressure. Hence, meaurements on cell were restricted in the range from 900 to 1250 K. The polarization effect was of the order on 1 mV for cell 2. By statistical analysis a mild non-linearity was detected in the variation of emf of cell 2 with temperature, although this is not apparent in the scale of **Figure 4**. The expressions for the emf obtained by least-squares regression analysis are:

$$E_1\ (\pm 0.96)\ /\ \mathrm{mV} = 1154.6 - 0.57445(T/\mathrm{K}) \qquad (2)$$

$$E_2\ (\pm 0.2)\ /\ \mathrm{mV} = 610.0 - 0.80402(T/\mathrm{K}) + 0.04415(T/\mathrm{K})\ln(T/\mathrm{K}) \qquad (3)$$

The reversible emf of cell 3 could be measured only at one temperature, 773 K. At lower temperatures the emf was not reversible on micro-coulometric titration of oxygen through the cell in opposite directions. At 773 K the cell emf was reversible but significantly negative (-20.4 mV) indicating that the decomposition pressure of MnO_2 to Mn_2O_3 is significantly above atmospheric. Beacuse of the danger of explosion, experiments were not attempted at higher temperatures.

From the emf of cell 1, the oxygen chemical potential corresponding to the biphasic equilibrium between nonstoichiometric MnO and essentially stoichiometric Mn_3O_4 can be calculated in the temperature range from 850 to 1400 K. For the reaction:

$$\{6 / (1-4x)\}\ Mn_{1-x}O + O_2 = \{2(1-x) /(1-4x)\}\ \alpha\text{-}Mn_3O_4 \qquad (4)$$

$$\Delta\mu_{O_2}\ (\pm 370) / \mathrm{J\,mol^{-1}} = \Delta G_4^{\circ} = -4FE_1 = -445606 + 221.70(T/\mathrm{K}) \qquad (5)$$

From the emf of cell 2, the oxygen chemical potential for the biphasic equilibrium involving Mn_3O_4 and Mn_2O_3 and standard Gibbs energy change for the reaction,

$$4\ Mn_3O_4 + O_2 = 6\ Mn_2O_3 \quad (6)$$

$$\Delta\mu_{O_2}\ (\pm 77)\ /\ \mathrm{J\,mol^{-1}} = \Delta G_6^{o} = -4\mathrm{F}E_2 = -235421 + 310.3T - 17.04T\ln T \quad (7)$$

are obtained in the temperature range from 900 to 1250 K. The emf of cell 3 was obtained only at 773 K. From the value of emf , – 20.4(±0.6) mV, the oxygen potential for the oxidation of Mn_2O_3 to MnO_2 and the standard Gibbs energy change for the reaction,

$$2\ Mn_2O_3 + O_2 = 4\ MnO_2 \quad (8)$$

$$\Delta\mu_{O_2}\ (\pm 232)\ /\ \mathrm{J\,mol^{-1}} = \Delta G_8^{o} = -4\mathrm{F}E_3 = 7873 \quad (9)$$

The measured oxygen chemical potentials and Gibbs energy changes for oxidation reactions will be discussed in comparison with some of the values reported in the literature in the following section on assessment of thermodynamic data.

4. ASSESSMENT OF THERMODYNAMIC DATA

4.1. Mn_3O_4 (Hausmannite)

Mn_3O_4 undergoes a first order phase transition from α phase, with Jahn-Teller distorted spinel structure, to β phase with cubic spinel structure at 1445 K. There is a eutectic between MnO and Mn_3O_4 at 1835 K. It has a very narrow homogeneity range, $0.5710 < X_O < 0.5717$.

4.1.1. Low-temperature heat capacity and entropy of α-Mn_3O_4 at 298.15 K

Millar /12/ measured the heat capacity of α-Mn_3O_4 in the temperature range from 72 to 305 K. In order to calculate the entropy at 298.15 K, it is necessary to integrate C_P^o/T as a function of temperature from 0 to 298.15 K. This requires extrapolation of experimental heat capacity data to 0 K, which is associated with some uncertainty (±3.4 J K^{-1} mol^{-1}). Millar /12/ reported a value of 149.5 J K^{-1} mol^{-1} for entropy of α-Mn_3O_4 at 298.15 K. Robie and Hemingway /13/ have measured low-temperature heat capacities of Mn_3O_4 between 5 and 380 K using a fully automated adiabatically shielded calorimeter. The transition from

ferri-magnetic to paramagnetic was found to occur at 43.12 K. Robie and Hemingway /13/ reported a value of 164.1(±0.2) J K^{-1} mol^{-1} for the standard entropy of α-Mn_3O_4 at 298.15 K. Chhor et al. /14/ measured the heat capacity of Mn_3O_4 in the temperature range from 10 to 310 K using an automated adiabatic calorimeter. Magnetic transition was found at 43.15 K. Chhor et al. /14/ reported a value of 167.1 J K^{-1} mol^{-1} for entropy of α-Mn_3O_4 at 298.15 K.

Compared in **Figure 5**, are the low temperature heat capacity reported by Robie and Hemingway /13/ and Chhor et al. /14/ in the transition region. Above 50 K there is good general agreement between these two sets of measurement. However, minor discrepancies can be observed at lower temperature. The shoulder on the ascending side of the heat capacity peak at 40.1 K found by Robie and Hemingway /13/ was not confirmed by Chhor et al. /14/. The maximum measured C_P^o values are 121.4 J K^{-1} mol^{-1} at 43.12 K according to Robie and Hemingway /13/ and 188.1 J K^{-1} mol^{-1} at 43.15 K according to Chhor et al. /14/. Robie and Hemingway /13/ did not assess the entropy associated with the transition. The entropy was estimated by Chhor et al. /14/ by interpolating the base line C_P^o variation between 10 and 50 K and integrating $(C_P^{Ex}/T)dT$ in this range. The molar entropy of Mn_3O_4 associated with magnetic transition was assessed as11.5 J K^{-1} mol^{-1} /14/. The data of Robie and Hemingway /13/ was analyzed by Chhor et al. /14/ to generate the entropy of magnetic transition as 8.5 J K^{-1} mol^{-1}.

The two recent measurements of low-temperature heat capacity of α-Mn_3O_4 /13,14/ are of equal caliber and it is difficult to differentiate between the two. Hence, an average value, 165.6 (±1.0) J K^{-1} mol^{-1}, is selected for the standard entropy of α-Mn_3O_4 at 298.15 K.

4.1.2 High-temperature heat capacity and heat content ($H_T^o - H_{298.15}^o$) of Mn_3O_4

The equation for heat capacity of α-Mn_3O_4 obtained in this study (Eq. 1) can be integrated to give ($H_T^o - H_{298.15}^o$) as a function of temperature. Southard and Moore /15/ measured high-temperature heat content or enthalpy increment ($H_T^o - H_{298.15}^o$) of Mn_3O_4 in the temperature range from 498 to 1769 K by drop calorimetry. Samples of Mn_3O_4 were dropped from a platinum-rhodium high temperature furnace into a copper block

calorimeter. Compared in **Figure 6**, are values of ($H_T^o - H_{298.15}^o$) measured by Southard and Moore /15/ with those calculated from heat capacity data obtained in this study for α-Mn_3O_4 . There is good agreement between both sets of data. The heat content data of Southard and Moore /15/ for β-Mn_3O_4 in the temperature range from 1445 to 1800 K can be adequately fitted by linear least-squares analysis to give the expression;

$$H_T^o - H_{298.15}^o \text{ / J mol}^{-1} = -75135.6 + 210.9(T/\text{K}) \qquad (10)$$

The expression can be differentiated to obtain heat capacity for Mn_3O_4 in this range**.** The tetragonal to cubic phase transition of spinel Mn_3O_4 at 1445 K is associated with an enthalpy change of 18.83 kJ mol^{-1}. Based on these data thermodynamic functions, $H_T^o - H_{298.15}^o$, S_T^o and $-(G_T^o - H_{298.15}^o)/T$ for Mn_3O_4 can be constructed as functions of temperature. These values are listed in Table 4 along with other data assessed in this study.

4.1.3 Third-law analysis

The third-law of thermodynamics provides a better method for deriving the enthalpy of formation from measurement of the corresponding Gibbs energy of formation measured at high temperatures than the second-law method. It allows the calculation of the formation enthalpy from each data point. If the same value is obtained for enthalpy of formation at a reference temperature from Gibbs energy of formation at different temperatures, then internal consistency of all the data used in the analysis is confirmed. The third-law method is based on knowledge of the absolute entropy of the reactants and products based on low-temperature heat capacity measurements and the third law. The third-law analysis of the high-temperature data on Gibbs energy of formation is based on the equation,

$$\Delta_r H^o_{298.15} = \Delta_r G^o(T) - \Delta(H_T^o - H_{298.15}^o) + T\{\Delta_r S^o_{298.15} + \Delta(S_T^o - S_{298.15}^o)\} \qquad (11)$$

where $(H_T^{\circ} - H_{298.15}^{\circ})$ for each phase can be calculated as $\int_{298.15}^{T} C_p^{\circ} dT$ and $(S_T^{\circ} - S_{298.15}^{\circ})$ can be calculated as $\int_{298.15}^{T} (C_p^{\circ}/T) dT$. The quantity $\Delta(H_T^{\circ} - H_{298.15}^{\circ})$ and $\Delta(S_T^{\circ} - S_{298.15}^{\circ})$ represent the difference of between the sum of these quantities for products and reactants multiplied by the appropriate stoichiometric coeffients (i); $\Sigma i(H_T^{\circ} - H_{298.15}^{\circ})$ and $\Sigma i(S_T^{\circ} - S_{298.15}^{\circ})$, respectively. $\Delta_r H^{\circ}_{298.15}$ is the derived standard enthalpy change for the specified reaction at 298.15 K and $\Delta_r G^{\circ}(T)$ is the measured standard Gibbs free energy change at temperature T. Values of $\Delta_r H^{\circ}_{298.15}$ can be derived from each value of free energy change. If the derived values and independent of the temperature of the free energy measurement, then all the data used for analysis are internally consistent and accurate.

4.1.4 Enthalpy of formation of Mn_3O_4 at 298.15 K

For assessing the enthalpy of formation of α-Mn_3O_4 at 298.15 K, consider the oxidation of stoichiometric MnO according to the reaction,

$$6\ MnO + O_2 = 2\ \alpha\text{-}Mn_3O_4 \qquad (12)$$

Measured value for the Gibbs energy change for this reaction is available only below 900 K when the nonstoichiometry of MnO becomes negligible. At higher temperatures, MnO contains excess of oxygen because of cation vacancies, and the oxidation reaction is best represented by reaction (4). Since auxiliary thermodynamic functions for nonstoichiometric $Mn_{1-x}O$ are not available, the best option is to compute standard free energy change for the hypothetical reaction (12) for temperatures higher than 900 K using measured oxygen potentials for the biphasic equilibrium and evaluated activity of MnO in $Mn_{1-x}O$ in equilibrium with Mn_3O_4.

For the evaluation of activity of MnO in $Mn_{1-x}O$, information on the variation of oxygen potential with nonstoichiometric parameter, x, is required. Using Gibbs-Duhem

equation, activity of Mn (a_{Mn}) at the oxygen-rich phase boundary of $Mn_{1-x}O$ ($X_{\mathrm{O}}^{\mathrm{s}}$) can be evaluated:

$$\log a_{\mathrm{Mn}} = \int_{X_{\mathrm{O}}=0.5}^{X_{\mathrm{O}}^{S}} -1/2(X_{\mathrm{O}} / X_{\mathrm{Mn}}) d \log P_{\mathrm{O_2}} \qquad (13)$$

Since stoichiometric MnO ($X_{\mathrm{O}} = 0.5$) is in equilibrium with pure Mn metal, $a_{\mathrm{Mn}} = 1$ at this boundary. The mole fraction of oxygen in $Mn_{1-x}O$ is related to the nonstoichiometric parameter: $X_O = 1/(2-x)$. The oxygen-rich compositions of $Mn_{1-x}O$, defined by the phase diagram, are listed in **Table 1**. Keller and Dieckmann /16/ measured values of x as a function of oxygen partial pressure (P_{O_2}) at regular intervals of temperature from 1173 to 1673 K. The values of the activities of Mn at oxygen-rich compositions at different temperatures are presented in **Table 2**. From the activity of Mn and oxygen potential at the oxygen-rich boundary, activity of MnO can be computed using accurately known value of Gibbs energy of formation of MnO /2/. For the reaction,

$$\mathrm{Mn} + 1/2\ \mathrm{O_2} = \mathrm{MnO} \qquad (14)$$

$$\Delta G^{\mathrm{o}}_{\mathrm{MnO}} = -RT \ln a_{\mathrm{MnO}} / a_{\mathrm{Mn}} + 0.5 \Delta \mu_{\mathrm{O_2}} \qquad (15)$$

The activities of MnO (a_{MnO}) in the oxygen-rich nonstoichiometric phase thus calculated at different temperatures are displayed in **Table 2**. Using this activity and the measured oxygen potentials for the biphasic equilibrium between $Mn_{1-x}O$ and Mn_3O_4, the standard Gibbs energy change for reaction (12) is computed at higher temperatures:

$$\Delta G^{\mathrm{o}}_{12} = 6\mathrm{R}T \ln a_{\mathrm{MnO}} + \Delta \mu_{\mathrm{O_2}} \qquad (16)$$

Since Mn_3O_4 is essentially stoichiometric, its activity is taken as unity. The calculated Gibbs energy changes for reaction (12) are also listed in **Table 2**.

For third-law analysis, auxiliary data { $S^{\mathrm{o}}_{298.15}$, $\Delta(H^{\mathrm{o}}_T - H^{\mathrm{o}}_{298.15})$ and $\Delta(S^{\mathrm{o}}_T - S^{\mathrm{o}}_{298.15})$ } for O_2 gas and solid MnO are needed. High temperature heat content $(H^{\mathrm{o}}_T - H^{\mathrm{o}}_{298.15})$, entropy increment $(S^{\mathrm{o}}_T - S^{\mathrm{o}}_{298.15})$ and standard entropy { $S^{\mathrm{o}}_{298.15}$ /

J K^{-1} mol^{-1} = 59.02 (±0.4)} of MnO were taken from a recent publication /2/ and the corresponding quantities for O_2 gas from JANAF thermochemical tables /17/ { $S^{o}_{298.15}$ / J K^{-1} mol^{-1} = 205.147 (±0.035)}. Using the selected standard entropy of Mn_3O_4 at 298.15 {165.6 (±1.5) J K^{-1} mol^{-1}}, the standard entropy change for reaction (12) at 298.15 K, ($\Delta_r S^{o}_{298.15}$) is –228.067 J K^{-1} mol^{-1}.

Third-law analysis of the results obtained in this study for the biphasic equilibrium between $Mn_{1-x}O$ and Mn_3O_4 was carried out with and without the correction for the activity of MnO. The correction is applied only at three temperatures, 1173, 1273 and 1373 K; the magnitude of the correction increases with temperature and nonstoichiometry. The results are shown in **Figure 7**. It is seen that without correction (filled symbol) the derived values of $\Delta_r H^{o}_{298.15}$ for reaction (12) show significant increase with temperature. However, when correction is applied $\Delta_r H^{o}_{298.15}$ is almost independent of temperature (open symbol) and yield the correct value for the enthalpy change.

There are numerous measurements on the oxygen potential corresponding to the oxidation of $Mn_{1-x}O$ to Mn_3O_4 using a variety of techniques with lesser accuracy. Since most of these have discussed and analyzed at length by Grundy et al. /1/, the discussion will not be repeated here. However, two among the better data sets are analyzed to show trends: data from Charette and Flengas /6/, and Schaefer /18/. The results of the third-law analysis of their results are also displayed in Figure 6. The trend in their results is similar to that seen with the data obtained in this study. Without correction, all the values of $\Delta_r H^{o}_{298.15}$ for reaction (12) increase significantly with temperature and nonstoichiometry. The results of Charette and Flengas /6/ yield a value for $\Delta_r H^{o}_{298.15}$, which is 1.63 kJ mol^{-1} more positive than the result obtained in this study. The results of Schaefer /18/ show a temperature dependent error in measurement since the value of $\Delta_r H^{o}_{298.15}$ appear to vary with temperature even after correction for the activity of MnO. Because of the use of buffer electrode, the result obtained in this study is considered more accurate that the value evaluated from the measurements and Charette and Flengas /6/. Hence, the

value $\Delta_{r(12)}H^{o}_{298.15} = -450.562$ kJ mol^{-1} is selected for reaction (12). Using transposed temperature drop calorimetry and drop solution calorimetry in lead borate melt at 977 K, Fritsch and Navrotsky /19/ determined a value of –441.4(±5.8) kJ mol^{-1} for reaction (12) through an indirect route. Since complete oxidation or reduction of the oxide samples dropped into the calorimeter at 997 K in air was assumed but not ascertained, the result is of doubtful accuracy.

Enthalpy of formation of Mn_3O_4 can be calculated from this value and enthalpy of formation of MnO /2/:

$$\Delta_{r(12)}H^{o}_{298.15} = 2\Delta_{f(Mn_3O_4)}H^{o}_{298.15} - 6\Delta_{f(MnO)}H^{o}_{298.15} \qquad (17)$$

The standard enthalpy of formation of Mn_3O_4 from elements thus obtained is $\Delta_{f(Mn_3O_4)}H^{o}_{298.15} = -1386.185$ kJ mol^{-1}, in fair agreement with solution calorimetric value of Shomate /19/. Comparison of selected data $\Delta_f H^{o}_{298.15}$ and $S^{o}_{298.15}$ for Mn_3O_4 with values available in the literature is presented in **Table 3**. The literature values are taken from calorimetric measurements /20,21/, assessments /1/ or compilations /22-24/. Assessment of Grundy *et al.* /1/ uses both thermodynamic and phase diagram inputs based on Thermo-Calc database and PARROT computational software. A heavy reliance on phase diagram information and the use of a physically unrealistic model for the liquid solution, slightly distorts the assessment of thermodynamic data. Combustion calorimetric value of Siemonsen /20/ for enthalpy of formation is significantly more negative than information from all other sources. This old value can now be discarded. Because of the high accuracy now achievable with solid-state electrochemical cells, phase-equilibrium calorimetry involving the "third-law" analysis has emerged as a competing tool to solution and combustion calorimetry for determining the standard enthalpy of formation of oxides at 298.15 K, when heat capacities of both products and reactants are known over the full range of temperature. The new results suggest a major revision in the value of standard entropy of Mn_3O_4 at 298.15 K given in standard compilations. Based on the basic thermodynamic data for Mn_3O_4 selected in this study, a table of refined data for Mn_3O_4 is prepared (**Table 4**). Thermodynamic properties are listed at regular intervals of temperature and at temperatures of all phase transitions for Mn and Mn_3O_4. Values given in **Table 4**

supersede those available in earlier compilations /22-24/ and a more recent assessment /1/. There are no data for manganese oxides in JANAF thermochemical tables /17/.

4.2 Mn_2O_3 (Bixbyite)

Orthorhombic α-Mn_2O_3 transforms to cubic β-Mn_2O_3 at 307.5 K. This oxide is essentially stoichiometric.

4.2.1 Low-temperature heat capacity and entropy of Mn_2O_3 at 298.15 K

King /25/ measured the heat capacity of Mn_2O_3 in the temperature range from 51 to 298.15 K. Anti-ferromagnetic to paramagnetic transition occurs at 79.4 K which makes the extrapolation of heat capacity to 0 K rather difficult. King /25/ reported a value of 110.5 J K^{-1} mol^{-1} for entropy of Mn_2O_3 at 298.15 K, with a probable uncertainty of ±2.4 J K^{-1} mol^{-1}. Robie and Hemingway /13/ have measured heat capacity of Mn_2O_3 between 5 and 349 K using a fully automated adiabatically shielded calorimeter. Their values are systematically greater than that of King /25/ by 0.5 per cent. A sharp λ-point corresponding to of anti-ferromagnetic to paramagnetic transition was seen at 79.45 K. A broad change in heat capacity was also observed at 307.5 K, which was attributed to orthorhombic to cubic transition. The transition was continuous, with no enthalpy of transition. Robie and Hemingway /13/ reported a value of 113.7(±0.8) J K^{-1} mol^{-1} for entropy of Mn_2O_3 at 298.15 K. Uncertainty in the extrapolation of heat capacity from 0 to 51 K by King /25/ accounts for a large part of the difference of 3.2 J K^{-1} mol^{-1} between values of standard entropy reported by King /25/ and Robie and Hemingway /13/.

4.2.2 High-temperature heat content ($H_T^o - H_{298.15}^o$) and heat capacity of Mn_2O_3

Orr /26/ reported high-temperature heat content ($H_T^o - H_{298.15}^o$) of Mn_2O_3 in the temperature range from 397 to 1351 K by drop calorimetry. Heat capacity at 298.15 K derived from this high temperature data do not agree with that obtained from low-temperature measurements, probably because of the broad hump in heat capacity at 307.5 K. To overcome this difficulty, Robie and Hemingway /13/ integrated their C_P^o between 298.15 and 325 K to obtain ($H_{325}^o - H_{298.15}^o = 2872$ J mol^{-1}), then subtracted this quantity

from each of the measurements of Orr /26/ to obtain $H_T^o - H_{325}^o$, which was fitted to a polynomial. Differentiation of the polynomial gave an expression for heat capacity in the temperature range from 325 to 1400 K:

$$C_P^o / \mathrm{J\,mol^{-1}\,K^{-1}} = 162.36 + 0.01211(T/\mathrm{K}) + 1.046\mathrm{x}10^6(T/\mathrm{K})^{-2} + 3.462\mathrm{x}10^{-6}(T/\mathrm{K})^2 - 1317.3(T/\mathrm{K})^{-1/2} \quad \ldots\ldots(18)$$

This equation joins smoothly with the heat capacity measurements of Robie and Hemingway /13/. Graphically integrating C_P^o / T as a function of temperature one obtains $S_{325}^o - S_{298.15}^o = 9.24$ J K^{-1} mol^{-1}.

4.2.3 Enthalpy of formation of Mn_2O_3 at 298.15 K

The third-law analysis of the oxygen potential (Eq. 7) corresponding to the biphasic equilibrium between Mn_3O_4 and Mn_2O_3 can be used to derive enthalpy of formation of Mn_2O_3. For this analysis, auxiliary data on O_2 gas and Mn_3O_4 are also needed. Data for O_2 gas from JANAF thermochemical tables /17/ and for Mn_3O_4 from **Table 4** are used. Using the selected standard entropy of Mn_2O_3 at 298.15 {113.7 (±0.2) J K^{-1} mol^{-1}}, the entropy of change for reaction (6) is obtained: $\Delta_{r(6)} S_{298.15}^o = -185.35$ J K^{-1}mol^{-1} .

Results of third-law analysis of free energy data for reaction (6) is presented in **Figure 8**. The results from three sets of high temperature data are reasonably concordant. However, data of Charette and Flengas /6/ and Schaefer /18/ shows systematic increase in the derived value of $\Delta_{r(6)} H_{298.15}^o$ with temperature, suggesting possible temperature dependent errors in their measurements. Nevertheless, the mean values from their study connect well with the constant value of $\Delta_{r(6)} H_{298.15}^o$ obtained in this study**.** In view of this, $\Delta_{r(6)} H_{298.15}^o = -224.477$ kJ mol^{-1} is selected. Transposed temperature and drop calorimetric studies of Fritsch and Navrotsky /19/ suggest a value of – 201.8(±8.7) kJ mol^{-1}. As discussed earlier there is uncertainty regarding the completion of oxidation/reduction reactions during the course of their calorimetric measurement. Enthalpy of formation of

Mn_2O_3 from elements can be derived from the value and enthalpy of formation of Mn_3O_4 assessed in the study:

$$\Delta_{r(6)}H^{o}_{298.15} = 6\Delta_{f(Mn_2O_3)}H^{o}_{298.15} - 4\Delta_{f(Mn_3O4)}H^{o}_{298.15} \quad (19)$$

Thus, the enthalpy of formation of Mn_2O_3, $\Delta_{f(Mn_2O_3)}H^{o}_{298.15} = -961.536(\pm 1.0)$ kJ mol^{-1}.

Comparison of selected data $\Delta_f H^{o}_{298.15}$ and $S^{o}_{298.15}$ for Mn_2O_3 with values available in the literature is presented in **Table 5**. The literature values are taken from calorimetric measurements /20/, assessment /1/ or compilations /22-24/. As in the case of Mn_3O_4 combustion calorimetric value of Siemonsen /20/ for enthalpy of formation is significantly more negative than that obtained in this study. Based on the basic thermodynamic data for Mn_2O_3 selected in this study, a table of refined data for Mn_2O_3 is prepared (**Table 6**). Thermodynamic properties are listed at regular intervals of temperature and at temperatures of all phase transitions. Values given in **Table 6** supersede those available in earlier compilations /22-24/ and more recent assessment /1/.

4.3 MnO_2 (Pyrolusite)

There are several modifications of MnO_2. However, they are all metastable relative to the rutile form (space group $P4_2/mnm$).

4.3.1 Low-temperature heat capacity and entropy of MnO_2 at 298.15 K

Millar /12/ measured the heat capacity of MnO_2 in the temperature range from 72 to 294 K and calculated a value of 58.28(±1.4) J K^{-1} mol^{-1} for entropy of MnO_2 at 298.15 K by extrapolation to 0 K. Kelly and Moore /27/ also measured the heat capacity of MnO_2 using an adiabatic calorimeter in the temperature range from 55 to 295 K and calculated entropy of MnO_2 at 298.15 K as 53.14(±0.4) J K^{-1} mol^{-1}. In view of uncertainty in extrapolation of heat capacity to 0 K, the real uncertainty is probably ±1 J K^{-1} mol^{-1}. Robie and Hemingway /13/ measured the heat capacity of MnO_2 in the temperature range from 6 to 377 K using a fully automated adiabatically shielded calorimeter. Robie and Hemingway

/13/ reported a value of 52.75(±0.07) J K^{-1} mol^{-1} for entropy of MnO_2 at 298.15 K. Compared in **Figure 9**, are the low temperature heat capacity reported by Millar /12/, Kelly and Moore /27/ and Robie and Hemingway /13/. There is good general agreement between the different measurements. In the temperature range of 107 to 294 K heat capacity reported by Millar /12/ is slightly higher than those of Kelly and Moore /27/ and Robie and Hemingway /13/. The transition from anti-ferromagnetic to paramagnetic state occurs at Neel temperature T_N = 92.2 K.

4.3.2 High-temperature heat content ($H_T^o - H_{298.15}^o$) and heat capacity of MnO_2

Moore /28/ reported high-temperature heat content ($H_T^o - H_{298.15}^o$) of MnO_2 in the temperature range from 406 to 778 K by drop calorimetry. Robie and Hemingway /13/ integrated their C_P^o between 298.15 and 380 K to obtain enthalpy increment and combined with ($H_T^o - H_{298.15}^o$) values for MnO_2 between 406 and 778 K from Moore /28/. They fitted the combined data with a polynomial and then differentiated the expression to obtain the heat capacity in the temperature range from 298.15 to 850 K.

$$C_P^o / \mathrm{J\,mol^{-1}\,K^{-1}} = 290.41 - 0.14424(T/\mathrm{K}) + 2.0119\mathrm{x}10^6(T/\mathrm{K})^{-2} + 4.541\mathrm{x}10^{-5}(T/\mathrm{K})^2 - 3786.7(T/\mathrm{K})^{-1/2} \quad \text{.....(20)}$$

4.3.3 Enthalpy of formation of MnO_2 at 298.15 K

Compared in **Figure 10**, are values of the Gibbs energy change for reaction (8) reported by Klingsberg and Roy /29/ and Otto /30/ with that obtained in this study at 773 K. There is inconsistency in the data presented in Figure 1 and Table VI of Klingsberg and Roy /29/ at lower temperatures. Since the data in the figure are more extensive, they are plotted in **Figure 10.** At low temperatures, Gibbs energies for the reaction reported by two groups /29,30/ differ significantly, but at higher temperatures they converge. In this study Gibbs energy change for the reaction was measured at 773 K, which is significantly more negative than the data of Klingsberg and Roy /29/, but close to that of Otto /30/. The enthalpy change for reaction (8) is calculated from the measured Gibbs free energy change at 773 K (Eq. 9), by the third-law method. Using the selected standard entropy of MnO_2 at

298.15 {52.75 (±0.2) J K^{-1} mol^{-1}}, the standard entropy change for reaction (8), $\Delta_{r(8)}S^{o}_{298.15}$ is –110.77 J K^{-1} mol^{-1}. Auxiliary data on O_2 gas and Mn_2O_3 are from JANAF thermochemical tables /17/ and Table 6, respectively.

The enthalpy change for the reaction, $\Delta_{r(8)}H^{o}_{298.15}$, is obtained as –162.724(±3.0) kJ mol^{-1} in reasonable agreement with the value of –162.1**(**±7.2**)** kJ mol^{-1} suggested by Fritsch and Navrotsky /19/. In view of the large uncertainties associated with their values and concerns regarding the completion of reduction/oxidation reaction, the calorimetric measurements of Fritsch and Navrotsky /19/ are not very helpful in refining thermodynamic data for the higher oxides of manganese. Enthalpy of formation of MnO_2 from elements can be calculated as:

$$\Delta_{r(8)}H^{o}_{298.15} = 4\Delta_{f(MnO_2)}H^{o}_{298.15} - 2\Delta_{f(Mn_2O_3)}H^{o}_{298.15} \qquad (21)$$

Enthalpy of formation of MnO_2, $\Delta_{f(MnO_2)}H^{o}_{298.15}$, is – 521.449 (±0.9) kJ mol^{-1}.

Comparison of selected data $\Delta_f H^{o}_{298.15}$ and $S^{o}_{298.15}$ for MnO_2 with values available in the literature is presented in **Table 7**. The literature values are taken from calorimetric measurements /20,21/, assessment /1/ or compilations /22-24/. The value from combustion calorimetry of Siemonsen /20/ is again more negative than values obtained by others. The result computed in this study by the "third-law" method agrees well with solution calorimetric value of Shomate /21/. Based on the basic thermodynamic data for Mn_2O_3 evaluated in this study, a table of refined data for MnO_2 is prepared **Table 8**. Thermodynamic properties are listed at regular intervals of temperature and at temperatures of all phase transitions. As shown in **Figure 10**, the reassessed Gibbs free energy change for reaction (8) based on tables 6 and 8 agrees well the measurements of Otto /30/. Values for MnO_2 given in this **Table 8** supersede those available in earlier compilations /22-24/ and a more recent assessment /1/.

4. CONCLUSIONS

Since accurate thermodynamic data on higher oxides of manganese are required in metallurgy, ceramics and geology, they have been reassessed based on new measurements and critically selected information from the literature. The availability of accurate low-temperature heat capacity data /13,14/ allows precise definition of entropy. The entropy values are combined with new high-precision measurements on the chemical of oxygen in different biphasic regions of the system Mn-O using a sophisticated version of solid-state electrochemical cell, to generate accurate information on enthalpies of formation by applying the "third-law" method. This procedure, which may be called "phase-equilibrium calorimetry", now competes with direct calorimetry for determination of enthalpies of formation of oxides. Refined thermodynamic data for the three higher oxides of manganese, Mn_3O_4, Mn_2O_3 and MnO_2 are presented in tabular form at regular intervals of temperature and temperatures of phase transitions. The data now available in thermodynamic compilations /22-24/ require revision, especially for Mn_3O_4 and Mn_2O_3. The new assessed data for the higher oxides of manganese supplement improved information on MnO published earlier /2/.

ACKNOWLEDGEMENTS

G. Rajitha thanks the University Grants Commission of India for the award of Dr. D.S. Kothari Postdoctoral Fellowship, and K.T. Jacob acknowledges the Indian National Academy of Engineering for the award of their Distinguished Professorship.

REFERENCES

1. A.N. Grundy, B. Hallstedt and L.J. Gauckler, *J. Phase Equilib.*, **24**, 7-39 (2003).
2. K.T. Jacob, A. Kumar and Y. Waseda, *J. Phase Equilib.*, **29**, 222-230 (2008).
3. C.B. Alcock and S. Zador, *Electrochim. Acta*, **12**, 673-677 (1967).
4. J.N. Pratt, *Metall. Trans. A*, **21**, 1223-1250 (1990).
5. J. Fouletier, P. Fabry and M. Kleitz, *J. Electrochem. Soc*., **123,** 204-213 (1976).
6. G.G. Charette and S.N. Flengas, *J. Electrochem. Soc*., **115,** 796-804 (1968).
7. G.M. Kale, K.T. Jacob, *Metall. Trans. B*, **23,** 57-64 (1992).
8. K.T. Jacob and M. Attaluri, *J. Mater. Chem*., **13,** 934-942 (2003).
9. K.T. Jacob and R. Ranjani, *Mater. Sci. Eng. B*, (2011), doi: 10.1016/j.mseb.2011.01.012
10. T. Mathews and K.T. Jacob, *Appl. Phys. Lett.*, **57,** 511-513 (1990).
11. T. Mathews and K.T. Jacob, *Metall. Trans. A,* **23A**, 3325-3335 (1992)
12. R.W. Millar, *J. Am. Chem. Soc.*, **50**, 1875-1883 (1928).
13. R.A. Robie and B.S. Hemingway, *J. Chem. Thermodyn.*, **17**, 165-181 (1985).
14. K. Chhor, J.F. Bocquet C. Pommier and B. Chardon, *J. Chem. Thermodyn.*, **18**, 89-99 (1986).
15. J.C. Southard and G.E. Moore, *J. Am. Chem. Soc.*, **64**, 1769-1770 (1942).
16. M. Keller and R. Dieckmann, *Ber. Bunsenges. Phys. Chem.*, **89**, 883-893 (1985).
17. M.W. Chase, Jr, C.A. Davies, J.R. Downey, Jr, D.J. Frurip, R.A. McDonald and A.N. Syverud, JANAF Thermochemical Tables, *J. Phys. Chem. Ref. Data*, **14**, 1985
18. S.C. Schaefer, *Electrochemical Determination of Thermodynamic Properties of Manganomanganic Oxide and Manganese Sesquioxide*, Bureau of Mines Report of Investigations 8704, U.S. Department of the Interior, Washington, D.C., p. 1-17 (1982).
19. S. Fritsch and A. Navrotsky, *J. Am. Ceram. Soc.*, **79**, 1761-1768 (1996).
20. H. Siemonsen, *Z. Elektrochem. Angew. Phys. Chem.*, **45**, 637-643 (1939).
21. C.H. Shomate, *J. Am. Chem. Soc.*, **65**, 785-790 (1943).
22. D.D. Wagman, W.H. Evans, V.B. Parker, I. Halow, S.M. Bailey and R.H. Schumm, *Selected Values of Chemical Thermodynamic Properties, Tables for Elements 35*

Through 53 in the Standard Order of Arrangement, NBS Tech. Note 270-4, U.S. Department of Commerce, Washington, D.C., p. 106 (1969).

23. O. Knacke, O. Kubaschewski and K. Hesselman, *Thermodynamic properties of Inorganic Substances*, Springer-Verlag, Berlin, Germany, p. 1182-1185 (1991).
24. L.B. Pankratz, *Thermodynamic Properties of Elements and Oxides*, Bull. U.S. Bur. Mines, Bulletin 672, Washington, D.C., p. 229-236 (1982).
25. E.G. King, *J. Am. Chem. Soc.*, **76**, 3289-3291 (1954).
26. R.L. Orr, *J. Am. Chem. Soc.*, **76**, 857-858 (1954).
27. K.K. Kelly and G.E. Moore, *J. Am. Chem. Soc.*, **65**, 782-785 (1943).
28. G.E. Moore, *J. Am. Chem. Soc.*, **65**, 1398-1399 (1943).
29. C. Klingsberg and R. Roy, *J. Am. Ceram. Soc.*, **43**, 620-626 (1960).
30. E.M. Otto, *J. Electrochem. Soc.*, **112**, 367-370 (1965).

Table 1

Stability field of $Mn_{1-x}O$

T / K	Metal saturation boundary $X_O = 1/(2-x)$	Mn_3O_4 saturation boundary $X_O = 1/(2-x)$
1173	0.5	0.50168
1273	0.5	0.50279
1373	0.5	0.50581

Table 2

The standard Gibbs energy change for the reaction (12), 6 MnO + $O_2 \rightarrow$ 2 Mn_3O_4, computed from oxygen potential measured in this study with correction for activity of MnO

T / K	$\Delta\mu_{O_2}$ ($Mn_{1-x}O$ + Mn_3O_4)	$\ln a_{Mn}$	$\ln a_{MnO}$	$\Delta_r G^o$ / J mol^{-1}
1173	-185552	-21.20840	-0.01538	-186446
1273	-163382	-19.88873	-0.02512	-164972
1373	-141212	-18.76980	-0.04214	-144093

Table 3

Comparison of basic thermodynamic data for Mn_3O_4 selected in this study with values reported in the literature

Source	$\Delta_f H^o_{298.15}$ / kJ mol^{-1}		$S^o_{298.15}$ / J K^{-1} mol^{-1}	
	Value	Method	Value	Method
Siemonsen /20/	-1407.92(±0.8)	Combustion Calorimetry	---	---
Shomate /21/	-1387.62(±1.1)	Solution calorimetry	---	---
Millar /12/	---	---	149.5	Heat Capacity 70 to 300 K
Robie and Hemingway /13/	-1384.5(±1.4)	Assessment	164.1(±0.2)	Heat Capacity 5 to 380 K
Chhor *et al*. /14/	---	---	167.1(±0.5)	Heat Capacity 10 to 310 K
Grundy *et al.* /1/	-1382.74	Assessment	168.34	Assessment
Wagman *et al*. /22/	-1387.8	Compilation	155.7	Compilation
Knacke *et al*. /23/	-1386.1	Compilation	154.4	Compilation
Pankratz /24/	-1387.8	Compilation	155.7	Compilation
This study	-1386.185(±1.2)	Third-law Analysis	165.6 (±1.0)	Selected value

Table 4

Reassessed Thermodynamic Data for Mn_3O_4

T/K	C_p^o J K^{-1} mol^{-1}	$H_T^o - H_{298.15}^o$ J mol^{-1}	S_T^o J K^{-1} mol^{-1}	$-(G_T^o - H_{298.15}^o)/T$ J K^{-1} mol^{-1}	$\Delta_f H^o$ kJ mol^{-1}	$\Delta_f G^o$ kJ mol^{-1}
298.15	142.36	0	165.60	165.60	-1386.185	-1284.409
300	142.67	264	166.48	165.60	-1386.176	-1283.779
400	155.26	15215	209.41	171.37	-1385.372	-1249.751
500	163.75	31185	245.01	182.64	-1384.332	-1215.966
600	170.61	47911	275.48	195.63	-1383.264	-1182.394
700	176.72	65282	302.25	208.99	-1382.210	-1149.001
800	182.42	83241	326.22	222.17	-1381.159	-1115.755
900	187.88	101757	348.03	234.96	-1380.081	-1082.647
980	192.14	116958	364.20	244.86	-1379.150	-1056.369
980	192.14	116958	364.20	244.86	-1385.825	-1056.370
1000	193.19	120812	368.10	247.28	-1385.648	-1049.525
1100	198.41	140392	386.75	259.12	-1384.449	-1015.969
1200	203.56	160490	404.24	270.50	-1382.945	-982.538
1300	208.66	181102	420.73	281.42	-1381.121	-949.236
1360	211.71	193713	430.22	287.78	-1379.872	-929.462
1360	211.71	193713	430.22	287.78	-1386.232	-929.462
1400	213.74	202222	436.38	291.94	-1385.785	-915.903
1411	214.29	204576	438.06	293.07	-1385.713	-912.238
1411	214.29	204576	438.06	293.07	-1391.353	-912.240
1445	216.01	211891	443.18	296.54	-1391.195	-900.813
1445	210.90	229615	455.43	296.53	-1373.471	-900.788
1500	210.90	241214	463.31	302.50	-1373.337	-882.651
1519	210.90	245222	465.96	304.53	-1373.442	-876.614
1519	210.90	245222	465.96	304.53	-1406.442	-876.612
1600	210.90	262304	476.92	312.98	-1406.393	-848.179
1700	210.90	283394	489.71	323.00	-1406.499	-813.289
1800	210.90	304484	501.76	332.60	-1406.651	-778.391

Table 5

Comparison of basic thermodynamic data for Mn_2O_3 selected in this study with values reported in the literature

Source	$\Delta_f H^o_{298.15}$ / kJ mol^{-1}		$S^o_{298.15}$ / J K^{-1} mol^{-1}	
	Value	Method	Value	Method
Siemonsen /20/	-973.6(±1.3)	Combustion Calorimetry	---	---
King /25/	---	---	110.46(±2.1)	Heat Capacity 51 to 298 K
Robie and Hemingway /13/	-959.0 (±1.0)	Assessment	113.70(±0.2)	Heat Capacity 5 to 349 K
Grundy *et al.* /1/	-962.59	Assessment	112.1	Assessment
Wagman *et al*. /22/	-958.97	Compilation	110.45	Compilation
Knacke *et al*. /23/	-958.97	Compilation	110.45	Compilation
Pankratz /24/	-958.97	Compilation	110.45	Compilation
This study	-961.536(±1.0)	Third-law Analysis	113.70(±0.4)	Selected

Table 6

Reassessed Thermodynamic Data for Mn_2O_3

T/K	C_p^o J K^{-1} mol^{-1}	$H_T^o - H_{298.15}^o$ J mol^{-1}	S_T^o J K^{-1} mol^{-1}	$-(G_T^o - H_{298.15}^o)/T$ J K^{-1} mol^{-1}	$\Delta_f H^o$ kJ mol^{-1}	$\Delta_f G^o$ kJ mol^{-1}
298.15	109.4	0	113.70	113.70	-961.536	-884.475
300	109.8	203	114.38	113.70	-961.512	-883.998
400	108.4	10823	144.93	117.87	-960.818	-858.275
500	114.6	21978	169.79	125.84	-960.126	-832.719
600	120.0	33711	191.17	134.98	-959.359	-807.309
700	124.9	45959	210.04	144.38	-958.531	-782.033
800	129.3	58672	227.01	153.67	-957.646	-756.877
900	133.4	71813	242.48	162.69	-956.698	-731.839
980	136.6	82614	253.98	169.68	-955.869	-711.977
980	136.6	82614	253.98	169.68	-960.319	-711.978
1000	137.3	85353	256.75	171.39	-960.149	-706.820
1100	141.0	99271	270.01	179.76	-959.071	-681.537
1200	144.6	113552	282.43	187.80	-957.778	-656.365
1300	148.0	128183	294.14	195.54	-956.269	-631.302
1360	150.1	137127	300.87	200.04	-955.260	-616.425
1360	150.1	137127	300.87	200.04	-959.500	-616.424
1400	151.4	143157	305.24	202.98	-959.086	-606.242

Table 7

Comparison of data for MnO_2 selected in this study with values reported in the literature

Source	$\Delta_f H^o_{298.15}$ / kJ mol^{-1}		$S^o_{298.15}$ / J K^{-1} mol^{-1}	
	Value	Method	Value	Method
Siemonsen /20/	-524.67(±4.2)	Combustion Calorimetry	---	---
Shomate /21/	-521.49(±0.8)	Solution Calorimetry	---	---
Millar /12/	---	---	58.28	Heat Capacity 97 to 294 K
Kelly and Moore /27/	---	---	53.14(±0.4)	Heat Capacity 54 to 295 K
Robie and Hemingway /13/	-520.7(±0.7)	Assessment	52.75(±0.07)	Heat Capacity 6 to 377 K
Grundy *et al.* /1/	-520.48	Assessment	53.95	Assessment
Wagman *et al*. /22/	-520.03	Compilation	53.05	Compilation
Knacke *et al*. /23/	-522.04	Compilation	53.14	Compilation
Pankratz /24/	-520.03	Compilation	53.05	Compilation
This study	-521.449(±0.9)	Third-law Analysis	52.75(±0.2)	Selected

Table 8

Reassessed Thermodynamic Data for MnO_2

T/K	C_p^o J K^{-1} mol^{-1}	$H_T^o - H_{298.15}^o$ J mol^{-1}	S_T^o J K^{-1} mol^{-1}	$-(G_T^o - H_{298.15}^o)/T$ J K^{-1} mol^{-1}	$\Delta_f H^o$ kJ mol^{-1}	$\Delta_f G^o$ kJ mol^{-1}
298.15	54.77	0	52.75	52.75	-521.449	-466.405
300	54.95	102	53.09	52.75	-521.450	-466.064
400	63.22	6038	70.11	55.02	-521.220	-447.620
500	68.34	12639	84.82	59.54	-520.615	-429.286
600	71.21	19632	97.56	64.84	-519.895	-411.088
700	72.68	26835	108.66	70.33	-519.216	-393.009
800	73.34	34140	118.42	75.74	-518.659	-375.018

Figure Captions

Fig. 1 Schematic diagram of the apparatus used for oxygen chemical potential measurements in three biphasic regions of the system Mn-O. The solid-state electrochemical cell has a buffer electrode that prevents polarization of the measuring electrode.

Fig. 2 Heat capacity of Mn_3O_4 measured using DSC. The curve represents the fitted equation.

Fig. 3 Temperature dependence of the emf of cell 1.

Fig. 4 Temperature dependence of the emf of cell 2.

Fig. 5 Comparison of low-temperature heat capacities of α-Mn_3O_4 reported by Robie and Hemingway /13/ and Chhor *et al*. /14/.

Fig. 6 Comparison of the enthalpy increment $(H_T^{\circ} - H_{298.15}^{\circ})$ of α-Mn_3O_4 reported by Southard and Moore /15/ with values calculated from C_P° measured in this study as a function of temperature. Experimental data for β-Mn_3O_4 can be represented by a linear relation.

Fig. 7 Results of "third-law" analysis of Gibbs energy of formation of Mn_3O_4 from MnO derived from oxygen potential measurements, with and without correction for the activity of MnO. The filled symbols represent values without correction and open symbols values with correction.

Fig. 8 Results of "third-law" analysis of Gibbs energy of formation of Mn_2O_3 from Mn_3O_4.

Fig. 9 Comparison of low-temperature heat capacity of MnO_2 reported by Millar /12/, Kelly and Moore /27/, and Robie and Hemingway /13/.

Fig. 10 Comparison of Gibbs energy change for the oxidation of Mn_2O_3 to MnO_2 reported by Klingsberg and Roy /29/, and Otto /30/ with the result obtained this study.

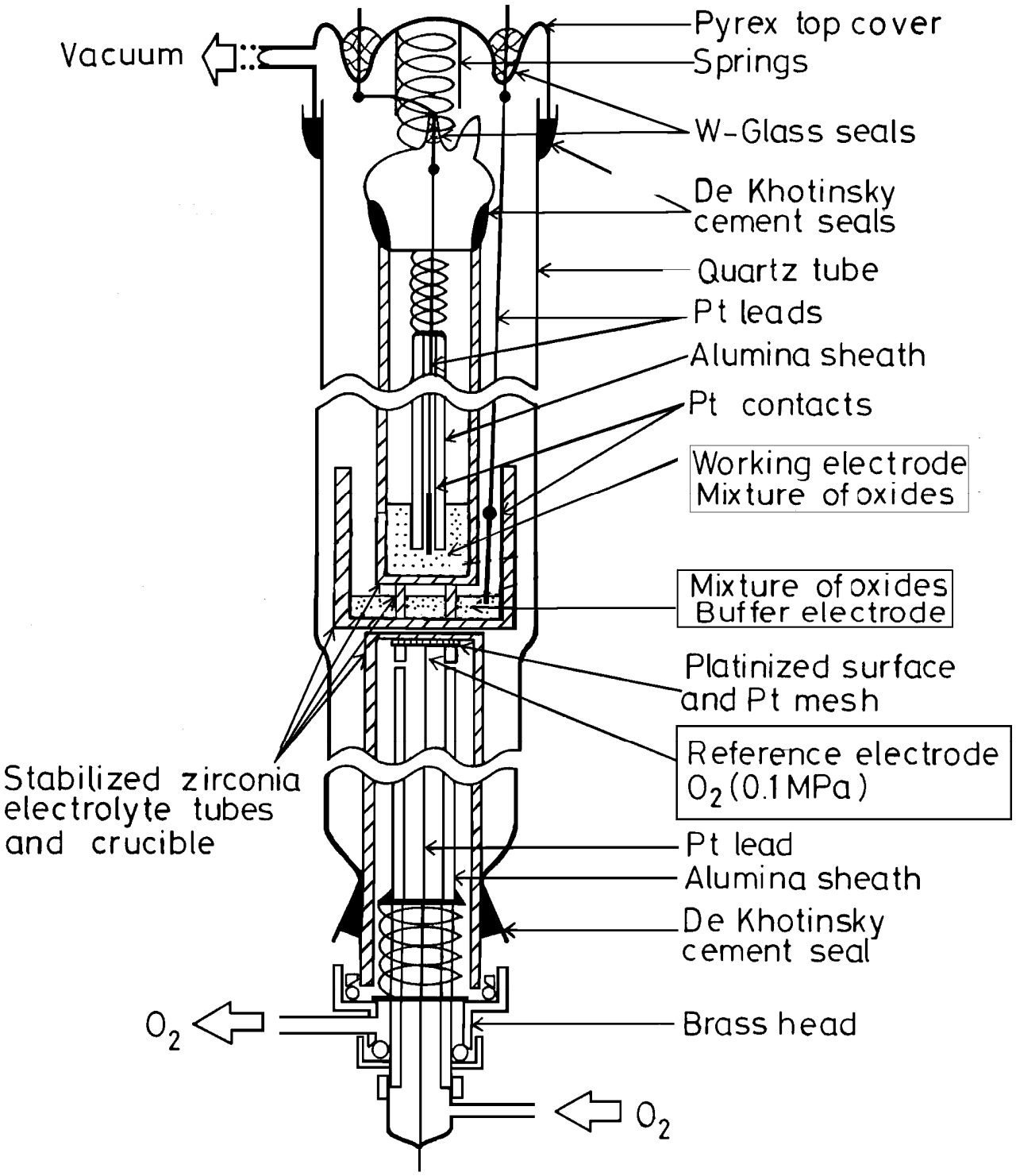
Vacuum
Pyrex top cover
Springs
W-Glass seals
De Khotinsky cement seals
Quartz tube
Pt leads
Alumina sheath
Pt contacts
Working electrode Mixture of oxides
Mixture of oxides Buffer electrode
Platinized surface and Pt mesh
Reference electrode O_2 (0.1 MPa)
Stabilized zirconia electrolyte tubes and crucible
Pt lead
Alumina sheath
De Khotinsky cement seal
O_2
Brass head
O_2

Figure 1

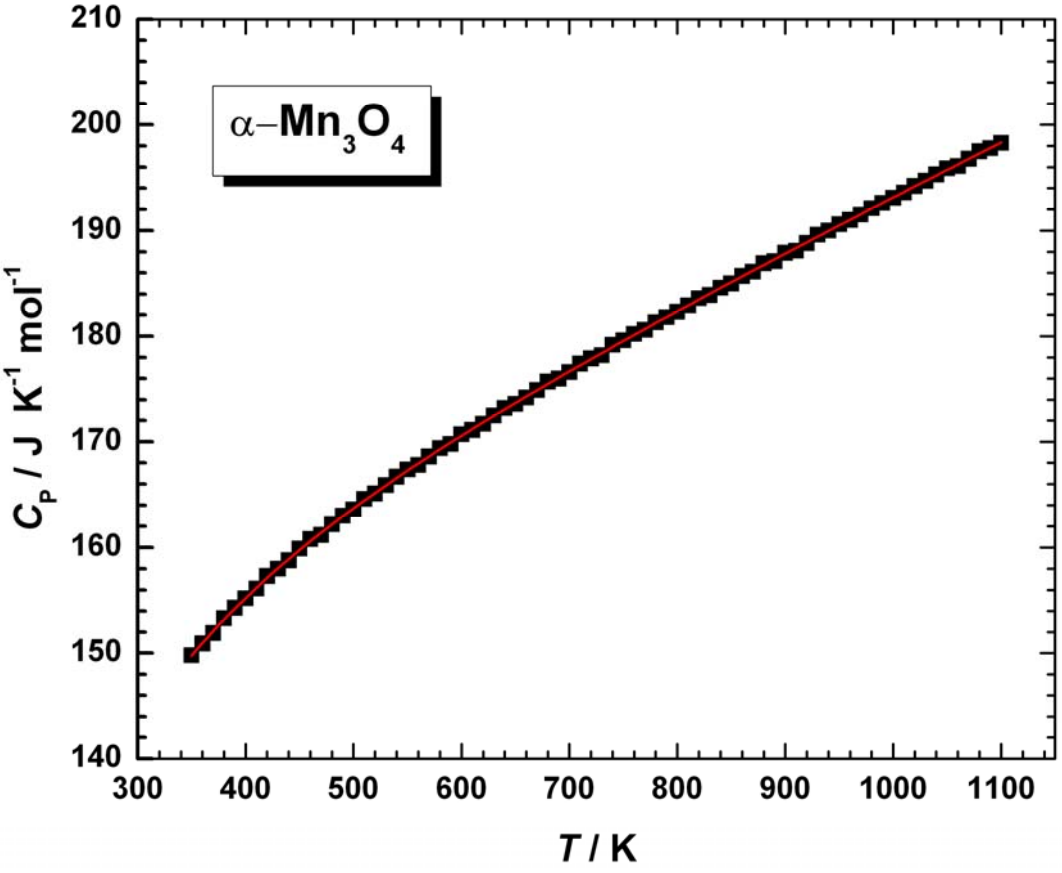
α–Mn3O4
210
200
190
180
170
160
150
140
300
400
500
600
700
800
900
1000
1100
Cp / J K-1 mol-1
T / K

Figure 2

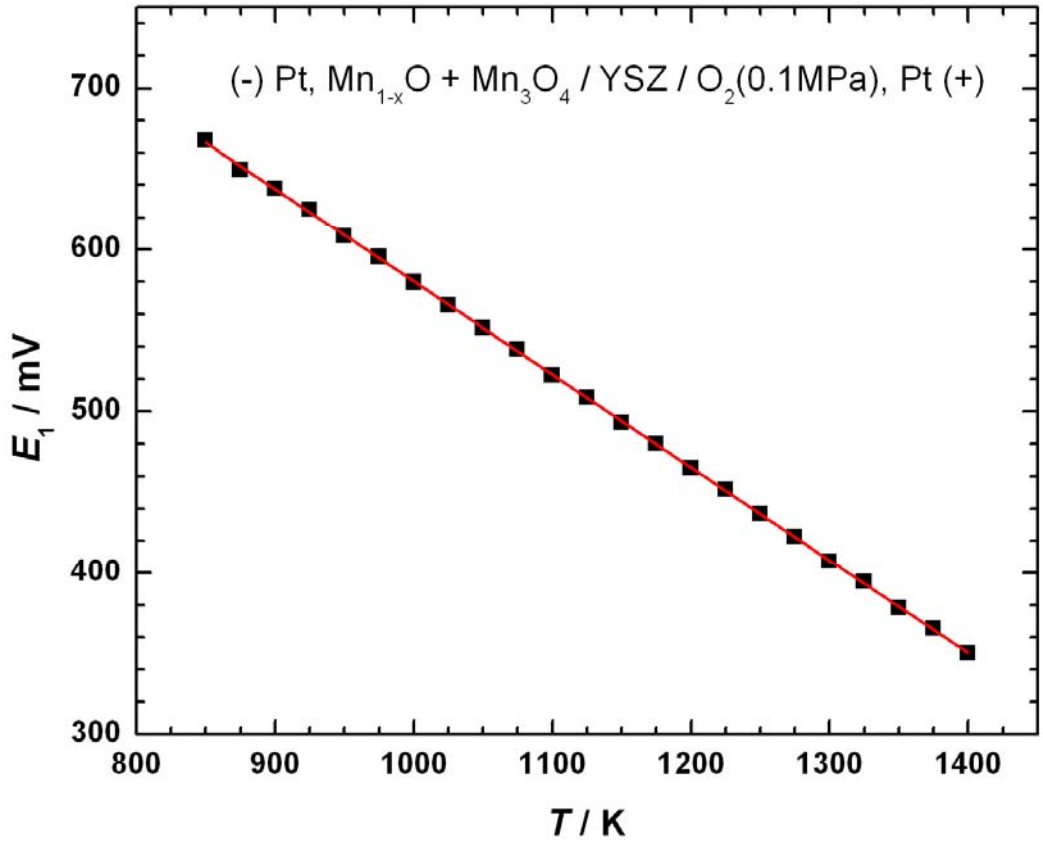
(-) Pt, Mn1-xO + Mn3O4 / YSZ / O2(0.1MPa), Pt (+)
E1 / mV
T / K
700
600
500
400
300
800
900
1000
1100
1200
1300
1400

Figure 3

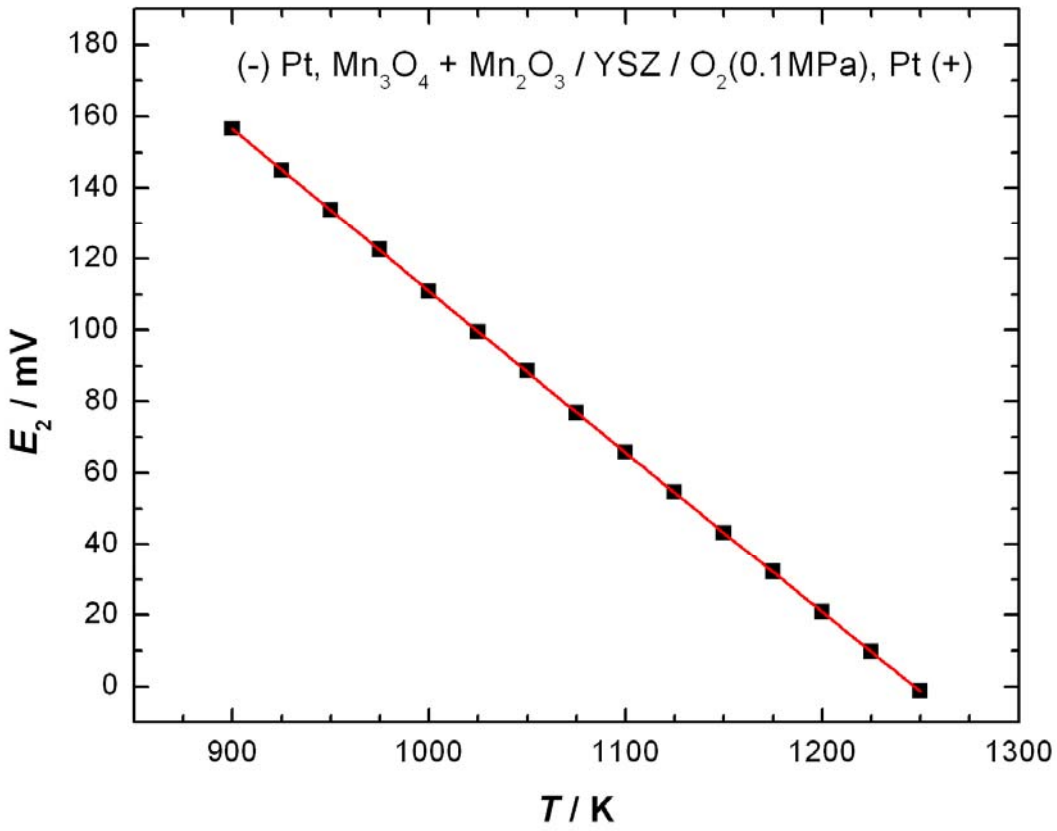
(-) Pt, Mn3O4 + Mn2O3 / YSZ / O2(0.1MPa), Pt (+)
E2 / mV
T / K
180
160
140
120
100
80
60
40
20
0
900
1000
1100
1200
1300

Figure 4

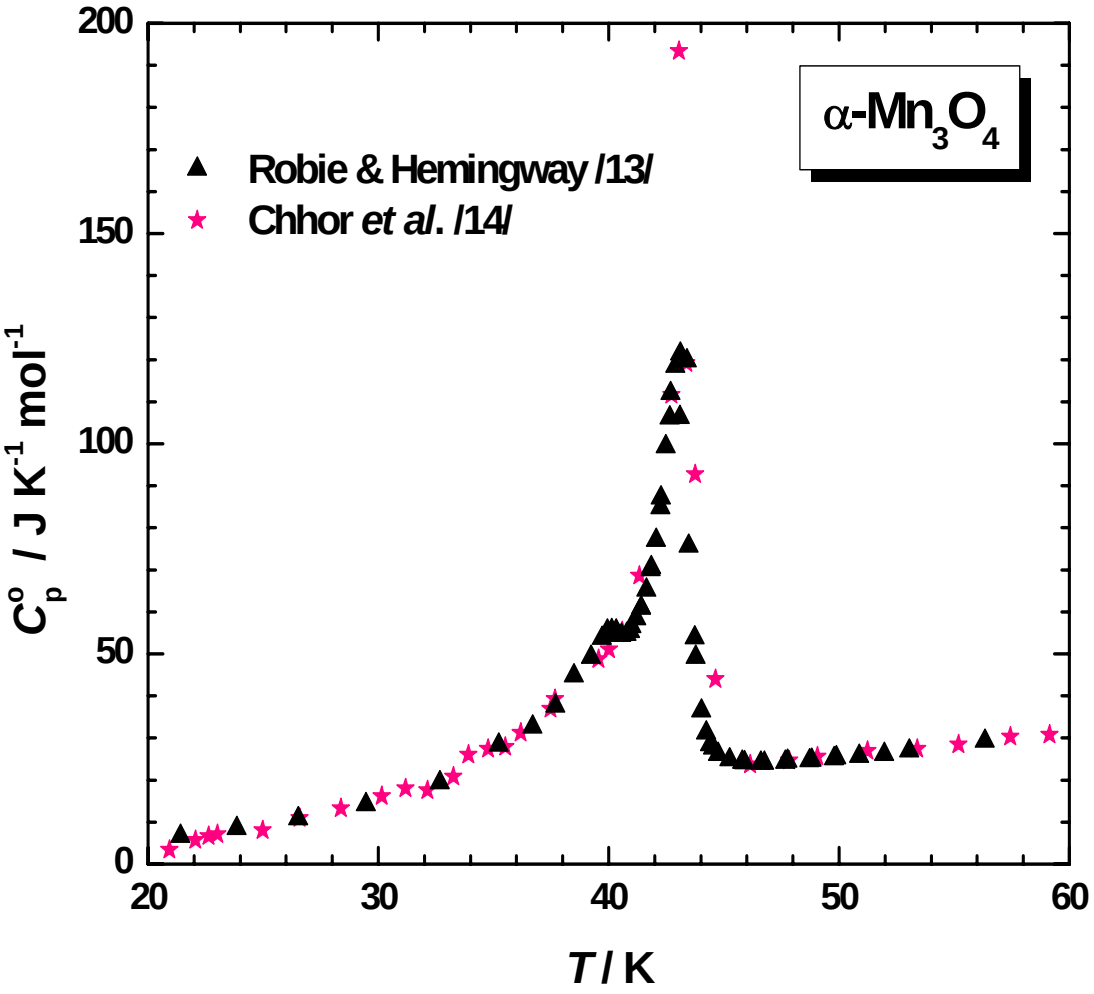
α-Mn3O4
Robie & Hemingway /13/
Chhor et al. /14/
Cp° / J K-1 mol-1
T / K
200
150
100
50
0
20
30
40
50
60

Figure 5

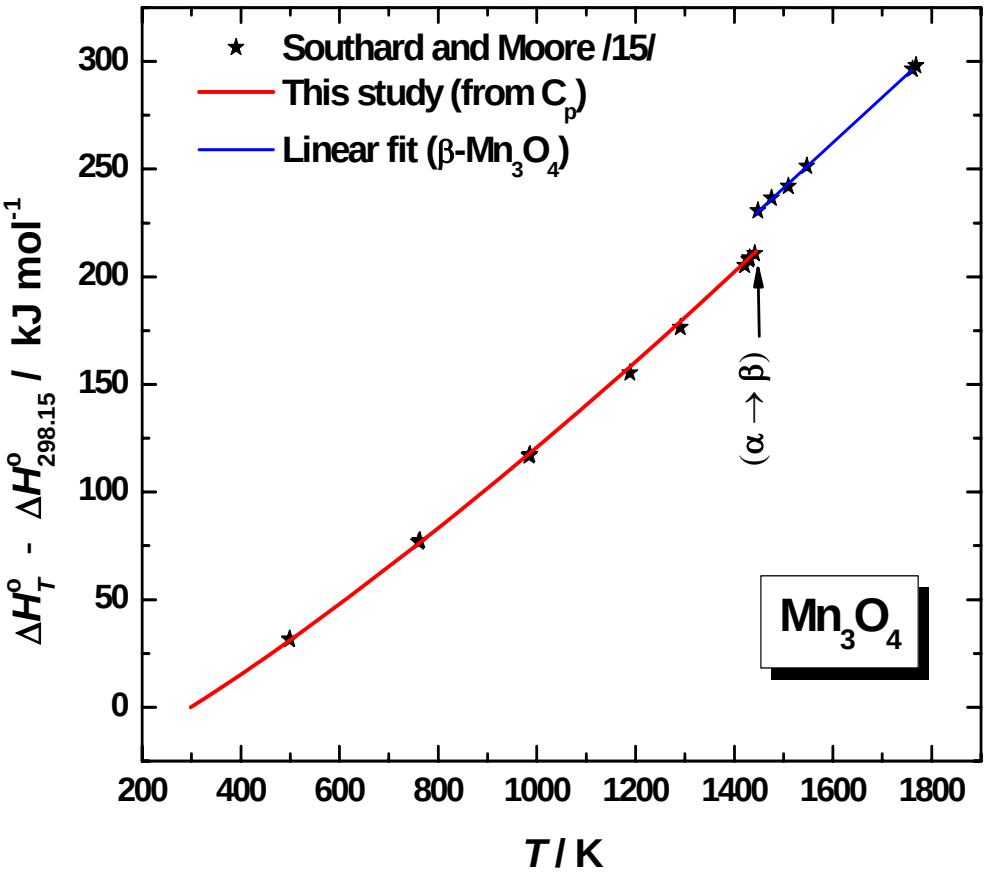
Southard and Moore /15/
This study (from C_p)
Linear fit (β-Mn_3O_4)
$(\alpha \rightarrow \beta)$
Mn_3O_4
$\Delta H^o_T - \Delta H^o_{298.15}$ / kJ mol^{-1}
T / K
0
50
100
150
200
250
300
200
400
600
800
1000
1200
1400
1600
1800

Figure 6

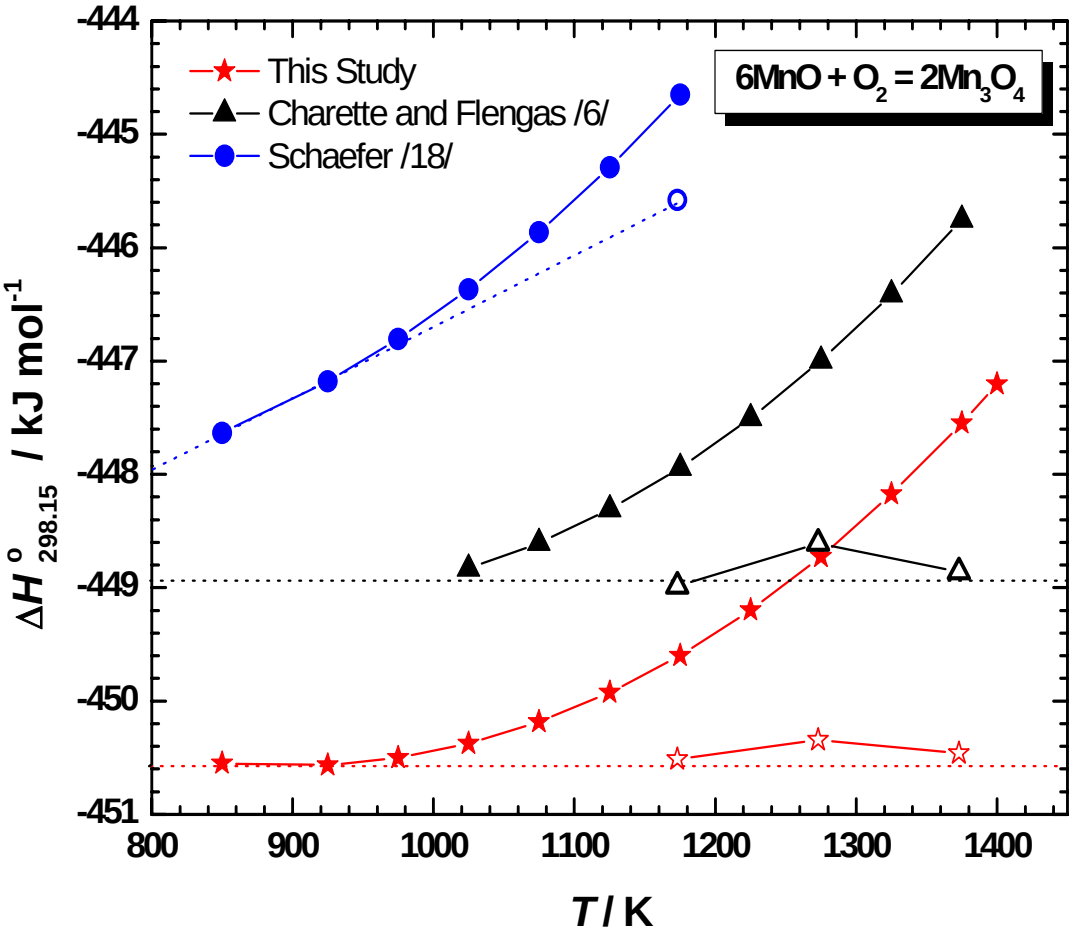
This Study
Charette and Flengas /6/
Schaefer /18/
6MnO + O2 = 2Mn3O4
ΔH° 298.15 / kJ mol-1
T / K
-444
-445
-446
-447
-448
-449
-450
-451
800
900
1000
1100
1200
1300
1400

Figure 7

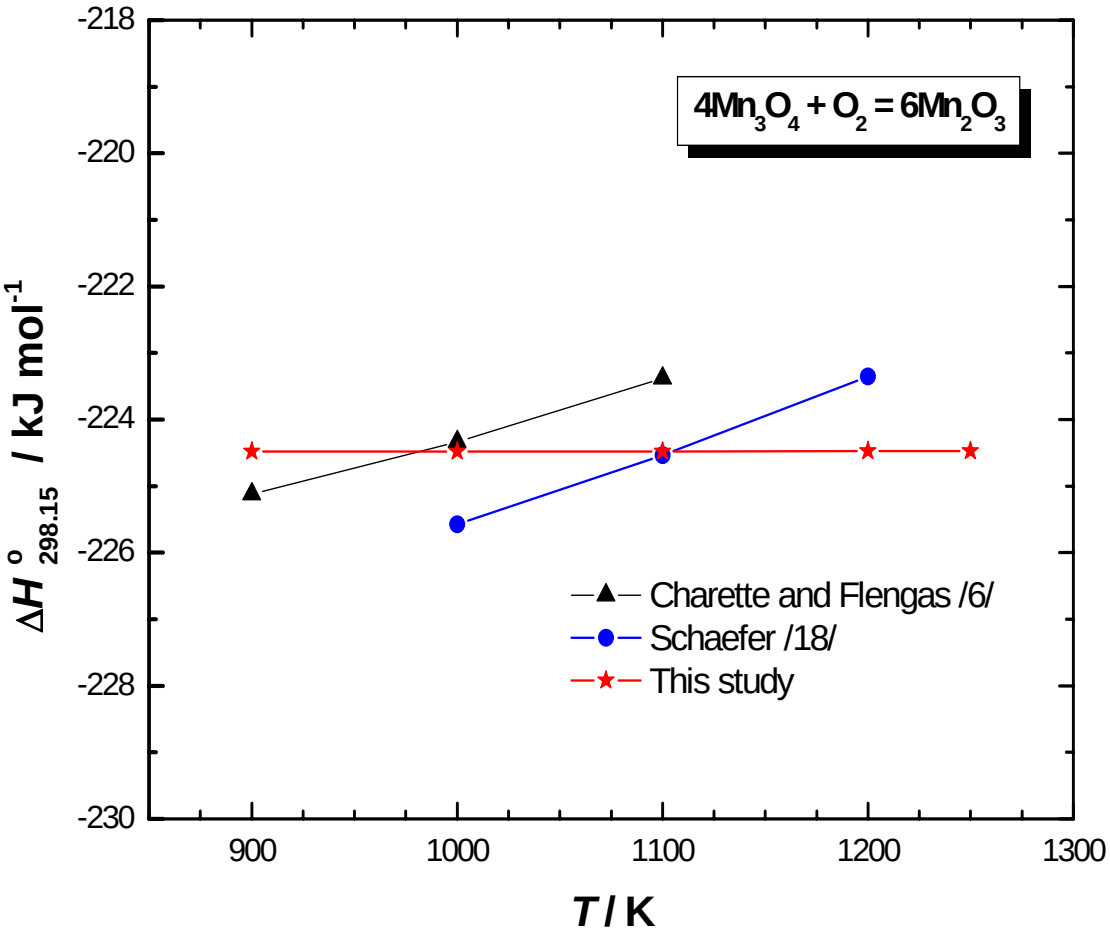
4Mn3O4 + O2 = 6Mn2O3
-218
-220
-222
-224
-226
-228
-230
900
1000
1100
1200
1300
ΔH° 298.15 / kJ mol-1
T / K
Charette and Flengas /6/
Schaefer /18/
This study

Figure 8

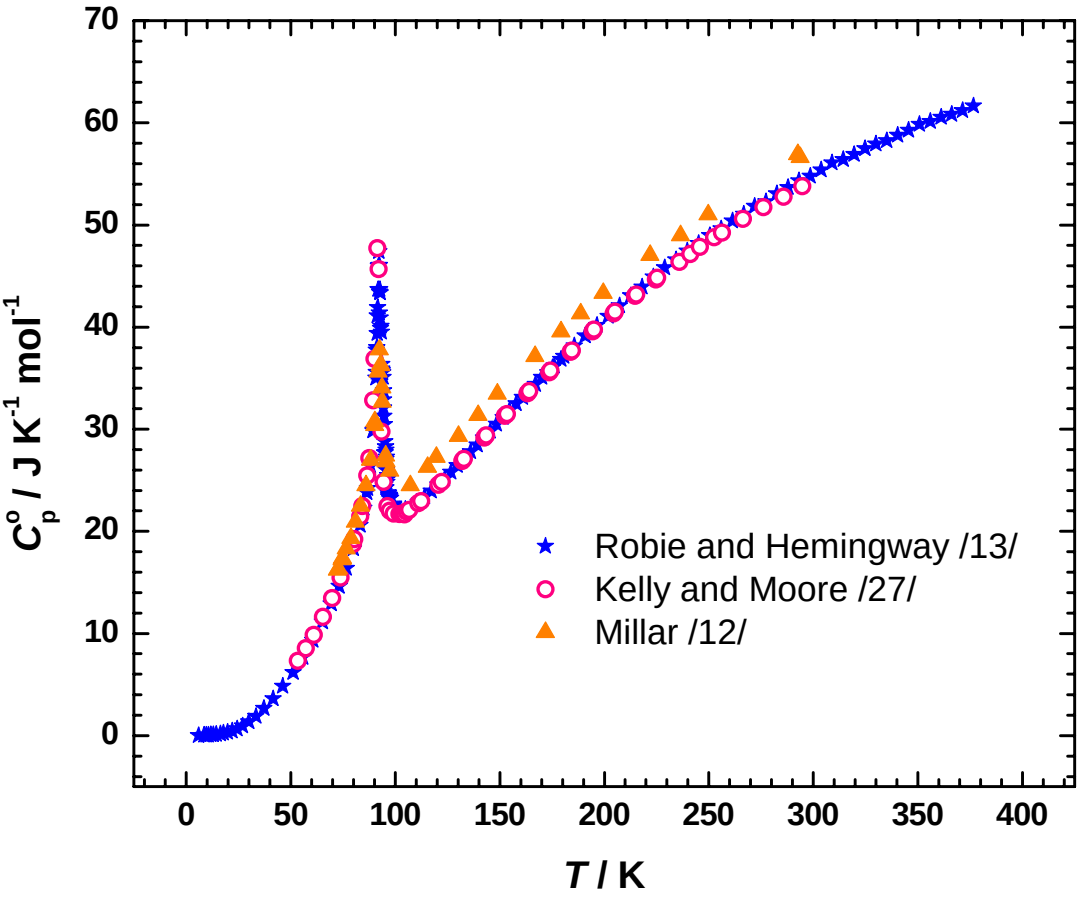
70
60
50
40
30
20
10
0
0
50
100
150
200
250
300
350
400
C_p^o / J K^{-1} mol^{-1}
T / K
Robie and Hemingway /13/
Kelly and Moore /27/
Millar /12/

Figure 9

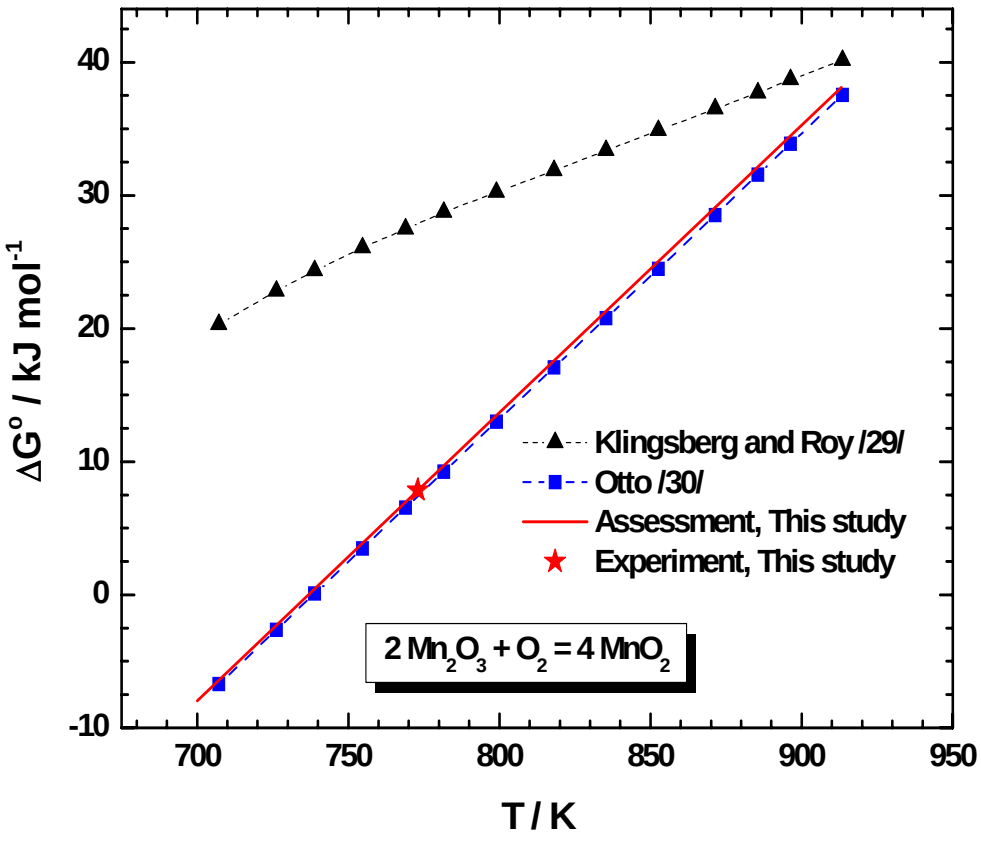
40
30
20
10
0
-10
700
750
800
850
900
950
ΔG° / kJ mol-1
T / K
Klingsberg and Roy /29/
Otto /30/
Assessment, This study
Experiment, This study
2 Mn2O3 + O2 = 4 MnO2

Figure 10